Published in final edited form as:
J Comp Physiol A Neuroethol Sens Neural Behav Physiol. 2010 April ; 196(4): 249–262. doi:10.1007/s00359-010-0511-y.

Electrophysiological properties of isthmic neurons in frogs revealed by *in vitro* and *in vivo* studies

Matthew S. Caudill[1,*], **Adam T. Eggebrecht**[1], **Edward R. Gruberg**[2], and **Ralf Wessel**[1]

[1] Department of Physics, Campus Box 1105, Washington University in St. Louis, Missouri 63130-4899, USA

[2] Department of Biology, Temple University, Philadelphia Pennsylvania 19122, USA

Abstract

The frog nucleus isthmi (parabigeminal nucleus in mammals) is a visually responsive, cholinergic and anatomically well-defined group of neurons in the midbrain. It shares reciprocal topographic projections with the ipsilateral optic tectum (superior colliculus in mammals) and strongly influences visual processing. Anatomical and biochemical information indicates the existence of distinct neural populations within the frog nucleus isthmi, which raises the question: are there electrophysiological distinctions between neurons that are putatively classified by their anatomical and biochemical properties? To address this question, we measured frog nucleus isthmi neuron cellular properties *in vitro* and visual response properties *in vivo*. No evidence for distinct electrophysiological classes of neurons was found. We thus conclude that, despite the anatomical and biochemical differences, the cells of the frog NI respond homogeneously to both current injections and simple visual stimuli.

Introduction

A striking feature of the vertebrate visual system is a bidirectional connectivity pattern linking higher and lower visual areas through a combination of both feedforward and feedback projections (Bullier 2006). Feedback projections have been shown to play a crucial role in the processing of visual information. In mammals for example, feedback projections from the cortex can alter the visual response properties of lateral geniculate nucleus neurons (Sillito et al. 2006) and modify the receptive fields of lower cortical neurons (Bullier 2006). In non-mammalian vertebrates such as amphibians, birds and reptiles, two electrophysiologically distinct types of feedback neurons in the nucleus isthmi (NI) (parabigeminal nucleus in mammals) differentially modulate responses of neurons in the optic tectum (OT) (superior colliculus in mammals), facilitating the selection of a single stimulus from an array of potential targets (Gruberg et al. 2006). In this paper, we address whether feedback neurons in the frog NI can be electrophysiologically differentiated into sets of distinguishable feedback projections that may serve distinct functional roles.

The isthmotectal system of non-mammalian vertebrates offers an advantageous substrate for understanding the roles played by feedback because the reciprocal connections between the OT and NI are well-isolated and topographically organized. In birds and reptiles, the NI is anatomically divided into sub-nuclei containing morphologically and biochemically distinct populations of neurons (Sereno and Ulinski 1987; Wang et al. 2004, 2006). These distinct

*mcaudill@physics.wustl.edu.

populations differentially influence the visual responsiveness of tectal neurons, possibly providing a mechanism for attention (Gruberg et al. 2006, Wang et al. 2000).

The frog NI, located ventral to the caudal pole of the OT (Fig. 1a,b), is composed of one anatomical nucleus, which contains two spatially segregated populations of neurons. Neurons located in the dorsolateral isthmi project to the ipsilateral OT, while neurons in the ventromedial isthmi project to the contralateral OT (Fig. 1c) (Dudkin et al. 2007). This bilateral pattern of connectivity is similar to the parabigeminocollicular connectivity of mammals (Jen et al. 1984; Tokunaga and Otani 1978). The ipsilateral feedback projections are topographically organized (Gruberg and Udin 1978), targeting among others, the dendritic columns of cholinergic layer 6 neurons in the OT from which they received inputs (Fig. 1c,d). Since retinal inputs are topographically arranged in the superficial tectum (Gaze 1958), these columns relay information from a specific region in visual space to the NI (Fig. 1c). In addition, neurons of the NI are further distinguished by the presence of acetylcholine (ACh) and gamma-aminobutyric acid (GABA) transmitters. Thus the NI of the frog, like birds and reptiles, may be suited to modulate neurons differentially at specific tectal locations, leading to feedback projections from the NI with distinct functional roles.

Here, we characterize both the cellular and visual response properties of NI neurons. Initially, we characterize the cellular properties of the isthmic neurons in response to somatic current injections *in vitro.* Then, we characterize the response properties of simultaneously recorded NI neurons around the tip of an extracellular recording electrode *in vivo* to visual stimuli.

Methods

Recording cellular properties *in vitro*

Surgery and Preparation—Six adult *Rana pipiens* (Northern Leopard frogs) (Hazen's Alburg, VT) were used in this portion of the study. All procedures used in this study were approved by the Washington University Institutional Animal Care and Use Committee and conform to the guidelines of the National Institutes of Health on the Care and Use of Laboratory Animals. Isthmic brain slices were obtained from adult leopard frogs that had been anesthetized by submersion in a 0.2% solution of 3-aminobenzoate methane-sulfonate salt (MS-222, Sigma, St. Louis, MO). After decapitation the brains were removed and placed in a Petri dish filled with ice-cold saline solution (pH = 7.4) composed of (in mM) 112 NaCl, 2 KCl, 3 $MgCl_2$, 17 $NaHCO_3$, 3 $CaCl_2$, and 24.2 glucose and saturated with 95% O_2 and 5% CO_2 (Yu and Debski 2003). This solution was also used as the bath solution in the recording chamber. The brain was then embedded in a 0.4% solution of low-melting-point agarose (type VII agarose, Sigma, St. Louis, MO, USA) and cooled until hardened. The embedded brain was sectioned at 300 μm on a tissue slicer (VF-200, Precisionary Instruments) in the transverse plane. Sections were collected and placed in the ice-cold saline and bubbled continuously with carbogen (95% O_2, 5% CO_2). The slice was then transferred to a recording chamber (RC-26G, Warner Instruments) mounted on a fixed-stage upright microscope equipped with differential interference contrast optics (BX-51WI, Olympus). The slice was held gently to the bottom of the chamber with an anchor of parallel nylon threads, and the chamber was perfused continuously with oxygenated saline at room temperature.

Recordings—Whole-cell recordings were obtained with glass micropipettes pulled from borosilicate glass (1.5 mm OD, 0.86 mm ID, AM Systems) on a horizontal puller (P-97, Sutter Instruments) and filled with a solution containing (in mM) 90 K-Gluconate, 25 NaCl, 12 HEPES, 1 CaCl2, 3 MgCl2 and 10 EGTA, and pH adjusted to 7.4 with KOH. Electrodes

were advanced through the tissue under visual guidance with a motorized micromanipulator (MP-285, Sutter Instruments) while constant positive pressure was applied and the electrode resistance was monitored by brief current pulses. Once the electrode had attached to a membrane and formed a seal, access to the cytosol was achieved by brief suction. Whole-cell recordings were performed with the amplifier (Axoclamp 2B, Axon Instruments) in the bridge mode (current clamp). Analog data were low-pass filtered (4-pole Butterworth) at 1 kHz, digitized at 5 kHz, stored, and analyzed on a PC equipped with a PCI-MIO-16E-4 and LabView software (both National Instruments).

Data Analysis—Despite the challenges associated with the small size of the frog NI neurons (diameter, 8 to 12 μm) (Li and Fite 2001), we obtained intracellular recordings for 8 NI cells from 6 animals with an average recording time of 20 minutes (range, 10–30 min). After obtaining a whole-cell patch seal, we measured passive, threshold, and above threshold membrane responses to 1-second current pulses. The membrane potential V_m (mV) was measured from the voltage trace 1 minute after the whole-cell configuration was achieved. The liquid junction potential was estimated to be approximately −9 mV using pCLAMP (Molecular Devices, Sunnyvale CA). This correction was ignored; i.e., the actual membrane potentials are more negative than the stated values. Each cell's input resistance R_{in} (MΩ) was calculated from the steady-state membrane potential responses to a small hyperpolarizing (-5 to -10 pA) 1-second current pulse. In addition, we fit an exponential to this voltage trace to determine the time constant of the membrane τ_m (ms). The rheobase current I_{Rh} (pA) was the smallest 1-second current pulse that elicited at least one action potential (AP). The rheobase latency T_{Rh} (ms) was the time difference between the onset of the rheobase current pulse and the peak voltage deflection of the first AP. To characterize the spike shapes, we determined the first-spike amplitude, the spike half-width and the after-hyperpolarization kinetics. The first-spike amplitude was the voltage difference between the peak amplitude of the AP and the peak amplitude in the after-hyperpolarization (AHP). The spike half-width was the width of the AP (ms) measured at half the maximum of the spike amplitude relative to rheobase voltage, which was estimated as R_{in}* I_{Rh}+V_m. The AHP time constant τ_{AHP} (ms) was calculated from a single-exponential decay fitting of the voltage trace following a single AP elicited at the rheobase current, fitting from the peak in the AHP to the steady-state voltage. Trains of APs were characterized by the interspike interval function and the relationship between the stimulus current and spike frequency. The time course of the interspike interval was measured from a response to a 1-second current pulse with amplitude of 90 pA. This current was chosen because it was well above the rheobase current for all cells. To quantify the spike-rate adaptation, the interspike interval data was fit with an exponential decay function, and the time constant τ_{SRA} (ms) and steady-state values $ISI_{Steady\text{-}State}$ (ms) were determined. To determine f-I curves, we counted the spikes elicited by a 1-second current pulse chosen from 10 to 100 pA in 10 pA steps in a pseudorandom sequence. In addition, the instantaneous frequency, defined as the inverse of the first interspike interval, was also calculated.

All numerical data gathered from cells is averaged and presented with standard deviations.

Principal Component Analysis—We used principal component analysis to assess whether the cells could be categorized into two or more populations based on their electrophysiological characteristics. Briefly, we standardized each of the measurements above by $\frac{x_i - \bar{x}}{\Delta\bar{x}}$, where x_i is a single measurement of one of the properties listed above, $\bar{x}$ is the average of all cells for a given property, and $\Delta\bar{x}$ is the standard deviation. The resultant parameters have a mean of zero and a normalized standard deviation with values between± 1.0. This normalization allows each parameter to contribute equally to the similarities and

differences among cells. Each of these values is an element in the correlation matrix of the data. We then determined the eigenvalues and eigenvectors of this correlation matrix using MATLAB 6.5 (Mathworks, Natick MA, USA) and projected the measured data onto the principal components (eigenvectors) with the largest eigenvalues.

Recording visual responses *in vivo*

Surgery and Preparation—Twenty-two adult *Rana pipiens* (Northern Leopard frogs) (Hazen's animal farm, Alburg, VT) were used in this portion of the study. Frogs were anesthetized by immersion in an aqueous solution of 0.2% 3-aminobenzoate methane-sulfonate salt (MS-222, Sigma, St. Louis, MO). Once fully anesthetized, a flap of skin was removed to expose the skull above the optic tectum, cerebellum, and the rostral part of the hindbrain. A rectangular patch of the exposed bone was removed with a Dremel drill with a 1-mm spherical bit. A small incision was then made into the dura mater, allowing the electrode direct access to a section of the brain underneath. Cotton was placed in the frog's mouth to push the eyes into the same configuration as in an awake and responsive frog. The frog was kept moist with a solution of 0.2% MS-222 in aquarium water dripped onto a gauze that snugly wrapped the frog. To ensure immobilization during recording, the frog was periodically injected with a 0.03 ml (per 20 grams body weight) solution of d-tubocurarine chloride (3 mg/ml; Sigma Co., St Louis) into the dorsal lymph sac.

The frog was secured to a rotatable stage and aligned with the recording electrodes and LCD monitor. The stage and electrodes were situated within a Faraday cage with a hole cut in the side, allowing the frog to see the visual stimulation monitor. The Faraday cage was covered in an opaque black conductive cloth to seal out ambient light.

Extracellular recordings—Borosilicate glass electrodes (A-M Systems, Everett, WA) were filled with Cerrolow-136 (Dowben and Rose 1953) and electroplated with gold and platinum to obtain impedances between 0.05 and 0.5 MΩ. The electrodes were placed into the frog's left NI through the OT with an motorized micromanipulator (MP 285, Sutter Instruments). Microelectrode locations were verified by an electrolytic lesion (−5 μA DC for 5 sec) at the recording site and visualized after fixing the tissue. The signal was amplified by a gain factor of 1,000 and filtered between 10 – 5,000 Hz with an A–M Systems 1800 amplifier. The signal was connected to a Tektronix TDS 210 oscilloscope and a speaker (AM Systems 3300) and monitored in real time. The signal was sent to the computer via a PC-LPM-16 data acquisition board (National Instruments, Austin, TX), acquired via LabVIEW (National Instruments, Austin, TX) with a sampling rate of 10 kHz, and stored off-line for later analysis. All data was analyzed off-line in MATLAB (Mathworks) with custom or built-in routines that are available upon request.

Histology—After the recording session, the frog was anesthetized with a 0.3% MS-222 solution and perfused through the conus arteriosus with a 0.7% NaCl solution followed by a fixative (75 ml 95% ethyl alcohol, 5 ml glacial acetic acid, 5 ml 37% formalin, 15 ml distilled water). The brain was removed and dehydrated through a graded set of alcohol solutions and cleared in cedarwood oil overnight. The brain was embedded in paraffin wax and sectioned transversely (thickness, 15 μm). Serial sections were floated onto albumen/glycerol coated slides covered with distilled water and dried thoroughly overnight on a slide warmer (at 40°C). The paraffin was dissolved in xylene (Sigma Co., St. Louis). The sections were hydrated, stained with cresyl violet (Sigma Co., St. Louis), and then dehydrated and coverslipped.

Visual stimulation—Once the electrode was placed in the NI, the stage was rotated to place the axis of the frog parallel to the stimulation monitor (Samsung 244T LCD monitor: contrast ratio of 1000:1, 24″, 1920 × 1200 resolution, 500 cd/m^2 maximum brightness). The frog's right eye was placed facing the monitor at a distance of 6 inches. The receptive fields were mapped out with a laser pointer or via the computer monitor with a white box on a black background or a black box on a white background (each controlled by a mouse). The center of the monitor was aligned with the center of the multi-unit receptive field. All stimuli were presented monocularly to the right eye.

The visual stimulation was presented via the Presentation software package (Neurobehavioral Systems, Albany, CA) with custom-built routines. The exact timing of the visual stimulus was reported in Presentation and checked with a photodiode. The response time of the monitor was 8 milliseconds. This lag is an order of magnitude smaller than the measured retinal latency and therefore did not influence the responses of the recorded neural units.

We presented two visual stimulations: flashes of diffuse illumination and moving spots. The diffuse illumination stimulus consisted of 5-seconds of a white screen at maximum brightness followed by a black screen. This protocol was repeated five times per trial. The moving-spot stimulus consisted of a spot appearing static on the screen in one of eight symmetric positions around the center of the receptive field. The spot was either 2° or 15° in diameter. After 3-seconds, the spot moved radially across the receptive field center to the opposite location at 10 deg/s. The spot then remained motionless on the opposite side of the screen for an additional 4 seconds before the trial ended.

Data Analysis—The acquired voltage signal was smoothed off-line by passing it through a band-pass filter between 300 and 5000 kHz formed with a 4-pole Butterworth filter. Spike events were detected using a threshold algorithm previously described (Eggebrecht 2009). The detected spike events were then sorted using a superparamagnetic clustering algorithm (Quiroga et al. 2004). Average firing rates were formed by binning the spike times into bins of 1 ms, averaging over trials, and convolving with an alpha function defined by $f(t)=\frac{t}{e^2}e^{-(\frac{t}{e})}$, where e is Euler's number and t is time (in ms). This function has a width at e_2 half-maximum of approximately 11 ms. To analyze the similarities and differences between the sorted unit responses, a principal component analysis was applied to several salient aspects of the responses observed in the temporal patterns of unit activity. Specifically, the salient aspects of the responses were computed by summing a unit's average firing rate during a period of time when a salient aspect was observed. We then divided this quantity by the total number of spikes within a complete trial to yield a normalized salient aspect. For the diffuse illumination, we chose the firing rates of the initial transient phase of the response, the secondary phase of activity, and the transient OFF phase of the response as three salient aspects for unit response comparisons. For the moving-spot stimuli, we chose the firing rates of the initial phase of the response at the commencement of motion and the delayed response at the cessation of motion for the two spot sizes along each of the eight movement directions. Thus, for the moving-spot stimuli, there were 32 salient response aspects used in the analysis. In addition, the spontaneous activity firing rate was also used as a salient aspect. Therefore, in total, 36 normalized salient aspects were obtained from the diffuse illumination, the moving-spot stimulus and the spontaneous activity. We pooled these 36 normalized salient aspects together before applying the principal component analysis. Briefly, we standardized each salient aspect (see in vitro data analysis) resulting in parameters with a mean of zero and a normalized standard deviation of ± 1.0. This normalization allows each parameter to contribute equally to the similarities and differences

among cells. As before, each of these values is an element in the correlation matrix of the data. We then determined the eigenvalues and eigenvectors of this correlation matrix using MATLAB 6.5 (Mathworks, Natick MA, USA) and projected the measured data onto the principal components (eigenvectors) with the largest eigenvalues.

In total, 48 recording sites in 22 frogs were utilized to obtain the data presented. At those sites, 152 units were well isolated from each other and the background noise. Of those, 80 units were tested with the entire set of stimulus varieties. These 80 units were used in the principal component analysis.

Results

Cellular properties

We performed intracellular recordings (in whole-cell patch mode) from 8 NI neurons in brain slices of 6 young adult *Rana pipiens* and analyzed their responses to somatic current injections (Fig. 2, 3). The locations of the recording sites (Fig. 2a) were distributed throughout the NI to including neurons projecting to the ipsilateral and contralateral OT. All recorded neurons displayed similar tonic discharge patterns in response to 1-second depolarizing current injections (Fig. 2).

Of the 8 neurons recorded, 6 had a resting membrane potential of −59 ± 7 mV and an input resistance of 1,007 ± 20 MΩ. The remaining 2 neurons were spontaneously spiking with mean rate of 2.5 Hz. The high input resistance we measured is consistent with small somata diameters ranging from 8 to 12 μm (Li and Fite 2001). The membrane time constant of the cells was 132 ± 23 ms. This time constant along with the input resistance gives membrane capacitances of 136 ± 35 pF (Fig 3a).

One consequence of the high input resistances of NI cells is that pico-ampere current injections bring the cells to threshold for spiking. We measured a rheobase current of 20 ± 4 pA with a first-spike latency of 294 ± 178 ms. The high variability in the first-spike latency is not due to outliers in the data set but to a broad distribution of data points (Fig. 3a). The rheobase current elicited an average of 1.8 spikes during the 1-second pulse. Measured relative to the trough in the AHP, the amplitude of the first spike was 69 ± 13 mV, and the spike half-width was 1.7 ± 0.4 ms. Following this first-spike, all cells displayed a monophasic AHP (Fig. 2b) with a time constant of 94 ± 46 ms. Although the standard deviation of τ_{AHP} is high, there is a smooth distribution of data points between the highest and lowest values recorded (Fig. 3a).

Current injections above the rheobase current elicited tonic discharge patterns that lasted the length of the 1-second stimulus pulse (Fig 2c). To characterize these discharge patterns, we measured the interspike intervals for currents between 10 and 100 pA for all cells and up to 150 pA for 3 of the cells. At low currents, the ISI curves show no spike-rate adaptation (Fig. 2d). However, for currents above 60 pA, a spike-rate adaptation was activated (Fig. 2e) that lasts the duration of the stimulus. For example, for a 90 pA current injection, the isthmic cells exhibited spike rate adaptation with a time constant of 29 ± 23 ms and a steady-state ISI value of 50 ± 15 ms. The variability in the data set is primarily attributed to one outlier in the data's distribution (Fig. 3a). We further characterized the tonic responses by counting the number of spikes during the 1-second stimulus pulse for current amplitudes between 10 and 100 pA. We found a linear relationship between spike frequency and current with slope of 0.27 Hz/pA (Fig. 2f).

Principal Component Analysis

The distribution of data measured across all cells is shown in figure 3a. Each column is a different measurement (see data analysis) and each colored circle represents the data from one cell. Some measurements do not have all 8 cells due to either spontaneous spiking or insufficient recording time to complete all ten measurements. To assess whether the data can be categorized into more than one group based on the cellular properties, we performed a principal component analysis (Jolliffe 1986) on the 6 cells (of the 8) that had sufficient recording time for all ten measurements. Using standardized variables we computed the eigenvalues of the correlation matrix (Fig. 3b inset) and determined for how much of the data's variance each eigenvalue accounts (Fig. 3b). We found that the first two eigenvalues account for 94% of the data's cumulative variance. This motivated our choice to keep only the first two principal components, reducing the parameter space to two dimensions. We projected the original data onto these two principal components (Fig. 3c). The principal component values for the 6 cells are scattered about the mean (zero in standardized variables), with no discrete clusters readily apparent. Thus, based on the distribution across each original parameter (Fig. 3a) and the principal component projection (Fig. 3c), our data suggest that the cellular properties of the NI neurons are homogeneously distributed.

Although the cellular properties suggest a homogeneous distribution of cell types, only 6 cells were available for this analysis. Therefore, we next considered the visual responses of many NI neurons *in vivo* to discern whether the NI contains electrophysiologically distinct populations. We employed multi-unit recording techniques in preference to single-unit recordings because the somata diameters of NI neurons are relatively small (8 to 12 μm) (Li and Fite 2001).

Visual Responses

Responses to visual stimulation *in vivo* were recorded at 48 locations within the NI in 22 *Rana pipiens* (Northern Leopard frogs). These locations were distributed throughout the NI, thoroughly sampling both the ipsilaterally-projecting dorso-lateral section of the NI and the contralaterally-projecting ventro-medial section of the NI. Here, we present only well-isolated single-unit activity sorted from multi-unit voltage traces. Our criteria for well-sorted spikes included well defined shapes with no kinks in the standard deviations (red lines, Fig. 4) and a refractory period in the interspike interval distribution of at least 2 ms (Fig. 4b–d).

Diffuse Illumination

In response to steps of diffuse illumination, the activity of units in the NI follow a characteristic temporal pattern (Fig. 5). By convolving the voltage traces (Fig. 5a) of responses to a 5-second flash with an alpha function, a clear pattern emerged in the multi-unit activity (Fig. 5b). These multi-unit responses were sorted (Eggebrecht 2009;Quiroga et al. 2004), resulting in 5 well-isolated single-units (Fig. 5c). For each unit, the time course of the response is characterized by five distinct phases that occur consistently in each of the 50 trials (only four rasters are shown for clarity). The first phase consists of bursts of activity that occur 80 to 120 ms after the stimulus is presented and last approximately 100 ms with an average maximum firing rate of 57.2 ± 9.8 Hz. The second phase is a suppression of activity that lasts for approximately 1500 ms. The average maximum firing rate of the units during this suppression phase is 0.7 ± 0.4 Hz, a value that is below the measured spontaneous rate of activity of 4.8 ± 2.3 Hz. This suppression of activity is noticeable in the raster plots and is consistent among the 5 sorted units. The third response phase is a broad increase in activity lasting for approximately 1 s with a peak average firing rate of 36.6 ± 10.8 Hz. The peak timing of this activity is consistent among the 5 sorted units. The fourth phase is a small increase in the average firing rate to 16.1 ± 4.2 Hz. In trials with longer

steps of illumination, this fourth phase of activity can persist for 2 s (data not shown). This phase is consistent among the 5 units and is visible in the raster plots of each unit. The fifth phase of activity is a delayed response to the OFF step change in illumination. This response occurs 80–120 ms after the stimulation has ceased, giving a delay that is consistent with stimulation onset delay. The average firing rate of the fifth phase is 43.1 ± 10.9 Hz. Despite the complexity of this temporal response to step changes in diffuse illumination, the consistency between the well-isolated single-units suggests that the responses of the NI neurons are homogeneous. Furthermore, we noted no differences between units in the ipsilaterally and contralaterally projecting regions of the NI. Thus, the time course of single-unit responses to step changes in illumination measured throughout the extent of the nucleus suggests that the NI contains a homogeneous population of neurons.

Moving-spot

To evaluate NI responses to spatiotemporal stimuli, we conducted 4 trials of dots moving radially through the multi-unit receptive fields of NI neurons. Specifically, we tested small and large black dots subtending 2-degrees and 15-degrees of visual space moving on a white background in 8 radial directions spaced 45-degrees apart. In each trial, the dot moved through the center of the receptive field at a speed of 10-degrees per second. The first 3 s of the responses (Fig. 6) and the last 4 s of the same responses (Fig. 7) are shown separately. As before, we convolved the multi-unit voltage trace (Fig. 6a and 7a) with the alpha function to determine the multi-unit average firing rate (Fig. 6b and 7b). We sorted the multi-unit voltage traces to find 5 well-isolated single-unit responses (Fig. 6c and 7c). While the responses of the units are varied and complex, there are several similarities among the responses of different units. First, all units undergo a transient increase in the firing rate 80–120 ms after the commencement of motion. The firing rate averaged across units is 81.8 ± 31.3 Hz, a value above the spontaneous rate of any given unit. Second, the average firing rate of the units remains elevated above the spontaneous rate for the duration of the stimulus movement. Third, no strong responses are seen at the cessation of motion following the typical latency of 80–120 ms (Blue box Fig. 7). Instead, a delayed response of 81.4 ± 41.4 Hz occurs 1700 ms after the cessation of motion. This delayed response is seen in all 5 sorted units. Taken together, these similarities in the temporal responses suggest that the responses of the NI neurons to spatiotemporal stimuli are homogeneous.

Principal Component Analysis of Visual Responses

To quantify the similarities and differences between unit activity in response to diffuse illumination and moving spots, we pooled the salient aspects from 80 well-isolated units recorded at 48 different isthmic locations. These salient aspects are normalized firing rates during specific phases of each unit's response (see methods). Histograms of three normalized salient aspects for the 80 units (Fig. 8) show a unimodal distribution of values about the average indicating that salient aspect responses obtained from different units at different isthmic locations are indistinguishable. Performing a principal component analysis on all salient aspects verified these initial findings. In particular, we determined that two principal components account for 87% of the variance in the salient aspect data across all 80 units. The projection of the data onto these two principal components (Fig. 9) yields a uniform distribution, indicating that the measured salient aspects from different units recorded at different locations are homogeneous. Thus, no distinction was found between unit responses to diffuse illumination and moving-spot stimuli. Instead, units in both the dorsal and ventral divisions of the NI respond homogeneously to simple visual stimuli.

Discussion

Many lines of evidence including neurotransmitter types, connectivity patterns and comparisons with other isthmotectal systems suggest that the NI of the frog contains electrophysiologically distinct classes of neurons. To address this hypothesis, we have characterized both the cellular properties and visual responses of isthmic neurons using both an *in vitro* and *in vivo* preparation. In the *in vitro* preparation we used whole-cell recordings to measure 10 variables that quantified the responses of NI neurons to current injection and applied a principal component analysis to expose any differences in the electrophysiological properties. We next used an *in vivo* preparation to measure the visual responses of single-units sorted from a extracellular multi-unit recordings in response to diffuse illumination and moving spot stimuli. We again applied a principal component analysis to examine similarities and differences in the responses of sorted single-units. Our results suggest that no distinction between putative cell types on the basis of their electrophysiological properties alone can be made. Instead, responses to both current injections and visual stimuli reveal a surprising homogeneity. To understand why this result is unexpected and its implications for the frog isthmotectal system we consider some of the lines of evidence that led to the hypothesis of distinct classes of frog NI neurons.

Neurotransmitters

Neurons in the NI of amphibians, reptiles and birds, as well as those of the parabigeminal nucleus (PBN) of mammals, all stain for acetylcholinesterase (AChE) and choline acetyltransferase (ChAT) (Wang 2003). In frogs, this cholinergic pathway can influence tectal cells and retinal inputs (Dudkin and Gruberg 2003). In addition, the NI has been shown to possess a population of GABA-containing neurons that project to the OT (Li and Fite 2001). This may account for the dual modulation of tectal cells observed when the NI is electrically stimulated (Hoshina et al. 2006; Xiao and Wang 1999). The homogeneity that we observed in both intracellular and extracellular recordings suggests two possible interpretations. One interpretation is that both the ChAT and GABA populations are indistinguishable on the basis of their responses to both current injections and simple visual stimuli such as diffuse illumination and moving spots. An alternative interpretation is that the GABA transmitter population is much smaller than the ACh transmitter population so the probability of recording from a GABAergic neuron is small.

Bilateral Connectivity Patterns

Anatomically, frog NI neurons are segregated into two spatially distinct groups; neurons in the dorsolateral region of the isthmi project to the ipsilateral OT, and neurons in the ventromedial region project to the contralateral OT but no single cell projects to both tectal lobes (Dudkin et al. 2007). A similar bilateral connectivity pattern is found in the parabigeminocollicular pathway of mammals such as cats, rodents and primates (Binns and Salt 2000; Cusick and Kaas 1982; Cynader and Berman 1972; Graybiel 1978; Künzle and Schnyder 1984; Mufson et al. 1986; Stevenson and Lund 1982; Wilson and Toyne 1970;). In rats for instance, the PBN (homolog of the NI) is divided into a dorsal, middle and ventral division (Jen et al. 1984; Tokunaga and Otani 1978). The dorsal and ventral divisions project to the ipsilateral superior colliculus (SC), and the middle division projects to the contralateral SC (Jen et al. 1984). The difference is that in cats some of the PBN cells projecting to the contralateral SC are much larger than the PBN cells projecting to the ipsilateral SC (Sherk 1979). In frogs, all cells in NI are about the same size. Despite the anatomical separation of cells in the frog NI, our results show that responses of cells in the dorsal and ventral divisions are indistinguishable. This homogeneity raises a fundamental question of why the NI neurons are spatially segregated into two divisions and may suggest

that interactions within and between the divisions play an important role in visual processing within the isthmotectal system. Further studies using multiple recording electrodes and pair-wise recordings would be suited to addressing these fundamental questions.

Comparisons with other isthmotectal systems

The frog NI is similar to other vertebrates' such as bony fish, reptiles and birds in that it makes reciprocal topographic projections with the ipsilateral OT (Gruberg et al. 2006). In goldfish the cells of the NI appear to be of one size and are richly interconnected by gap junctions (Williams et al. 1983) and appear to fire synchronously (Northmore and Gallagher 2003). However, in birds and reptiles, the NI consists of 2 or 3 sub-nuclei with electrophysiologically distinct populations of neurons. In birds, the subnuclei, the isthmi pars parvocellularis (Ipc) and the isthmi pars magnocellularis (Imc), can be differentiated by their responses to current injections, neurotransmitters, and cellular morphology. The cholinergic Ipc projects topographically in a narrow dorsoventral column in the OT while the GABAergic Imc projects to the OT anti-topographically (Wang et al. 2004, 2006). This spatial distribution allows the Imc and Ipc sub-nuclei to modulate tectal cells differentially, thereby enhancing responsiveness to salient visual targets (Gruberg et al. 2006; Wang 2003). In the frog, differential responses to NI stimulation have been extracellularly recorded throughout the OT layers (Xiao et al. 1999). The homogeneity of responses from the frog NI neurons in this study suggest that the NI population is electrophysiologically indistinguishable and implies that differential modulation of tectal cells may arise from interactions within the OT. This interpretation is partially supported by the recent ultrastructural studies that have shown that many isthmotectal axons targeting the contralateral OT terminate on GABA-immunoreactive dendrites (Rybicka and Udin 2005). Thus, it seems plausible that, in the frog, visual attention mechanisms may be mediated through inhibitory tectal interactions.

In summary, we have characterized the cellular and visual response properties of neurons in the frog NI. Our results show that despite differences in neurotransmitters, isthmic locations and comparisons with other isthmotectal systems, the responses of NI neurons are surprisingly homogeneous in terms of discharge patterns to current injections and responses to simple visual stimuli. While there is cell-to-cell variability in the measured cellular properties no distinction between cell types could be made. This was furthered by extracellular recordings which revealed that isthmic neurons responded similarly to simple visual stimuli.

Acknowledgments

We would to thank David Morton and Jeff Pobst for their critical reading of the manuscript. This work was supported by grant NIH-EY 15678 and NIH-EY 18818 to R. Wessel. All surgical procedures were approved by the Washington University Animal Care Facility and are in accordance with the National Institutes of Health guidelines on the Care and Use of Laboratory Animals.

Abbreviations

ACh	acetylcholine
ChAT	choline acetyltransferase
GABA	gamma-aminobutyric acid
Imc	isthmi pars parvocellularis
Ipc	isthmi pars parvocellularis

NI	Nucleus isthmi
OT	optic tectum
PBN	parabigeminal nucleus
SC	superior colliculus

References

Binns KE, Salt TE. The functional influence of nicotinc cholinergic receptors on the visual responses of neurons in the superficial superior colliculus. Vis Neurosci 2000;17:283–289. [PubMed: 10824682]

Bullier, J. What is Fed Back?. In: Van Hemmen, L.; Sejnowski, T., editors. 23 Problems in Systems Neuroscience. Oxford Univ. Press; New York: 2006. p. 103-132.

Cusick CG, Kaas JH. Retinal projection in adult and newborn grey squirrels. Brain Res 1982;256:275–284. [PubMed: 6179578]

Cynader M, Berman N. Receptive field organization of monkey superior colliculus. J Neurophysiol 1972;35:187–201. [PubMed: 4623918]

Dowben RM, Rose JE. A metal-filled microelectrode. Science 1953;118:22–24. [PubMed: 13076162]

Dudkin EA, Gruberg ER. Nucleus isthmi enhances calcium influx into optic nerve fiber terminals in *Rana pipiens*. Brain Res 2003;969:44–52. [PubMed: 12676363]

Dudkin EA, Sheffield JB, Gruberg ER. Combining visual information from the two eyes: The relationship between isthmotectal cells that project to ipsilateral and to contralateral optic tectum using fluorescent retrograde labels in the frog, *Rana pipiens*. J Comp Neurol 2007;502:38–54. [PubMed: 17335048]

Eggebrecht, AT. Dissertation. Washington University; Saint Louis: 2009. Mechanisms of feedback in the visual system.

Gaze RM. The representation of the retina on the optic lobe of the frog. Q J Exp Physiol 1958;43:209–214.

Graybiel AM. A satellite system of the superior colliculus: the parabigeminal nucleus and its projections to the superficial collicular layers. Brain Res 1978;145:365–374. [PubMed: 638795]

Gruberg E, Dudkin E, Wang Y, Marín G, Salas C, Sentis E, Letelier J, Mpodozis J, Malpeli J, Cui H, Ma R, Northmore D, Udin S. Influencing and interpreting visual input: The role of a visual feedback system. J Neurosci 2006;26:10368–10371. [PubMed: 17035519]

Gruberg ER, Udin SB. Topographic projections between the nucleus isthmi and the tectum of the frog *Rana pipiens*. J Comp Neurol 1978;179:487–500. [PubMed: 305927]

Hoshino N, Tsurudome K, Nakagawa H, Matusumoto N. Current source density analysis of contra-and ipsilateral isthmotectal connections in the frog. Vis Neurosci 2006;23:713–719. [PubMed: 17020627]

Jen LS, Dai ZG, So KF. The connections between the parabigeminal nucleus and the superior colliculus in the golden hamster. Neurosci Lett 1984;5:189–194. [PubMed: 6542631]

Jolliffe, IT. Principal component analysis. Springer-Verlag; New York: 1986.

Kunzle H, Schnyder H. The isthmus-tegmentum complex in the turtle and rat: a comparative analysis of its interconnections with the optic tectum. Exp Brain Res 1984;56:509–522. [PubMed: 6499978]

Li Z, Fite KV. GABAergic visual pathways in the frog *Rana pipiens*. Vis Neurosci 2001;18:457–464. [PubMed: 11497422]

Mufson EJ, Martin TL, Mash DC, Wainer BH, Mesulam MM. Cholinergic projections from the parabigeminal nucleus to the superior colliculus in the mouse: a combined analysis of horse radish peroxidase transport and choline acetyltransferase immunohistochemistry. Brain Res 1986;370:144–148. [PubMed: 3708316]

Northmore D, Gallagher S. Functionsal relationship between nucleus isthmi and tectum in teleosts: synchrony but no topography. Vis Neurosci 2003;157:453–465.

Quiroga RQ, Nadasy Z, Ben-Shaul Y. Unsupervised spike detection and sorting with wavelets and superparamagnetic clustering. Neural Comp 2004;16:1661–1687.

Rybicka KK, Udin SB. Connections of contralaterally projecting isthmotectal axons and GABA-immunoreactive neurons in *Xenopus* tectum: An ultrastructural study. Vis Neurosci 2005;22:305–315. [PubMed: 16079006]

Sereno MI, Ulinski PS. Caudal topographic nucleus isthmi and the rostral nontopographic nucleus isthmi in the turtle, *Pseudemys scripta*. J of Comp Neurol 1987;261:319–346. [PubMed: 3611415]

Sherk H. Connections and visual-field mapping in cat's tectoparabigeminal circuit. J Neurophysiol 1979;42:1656–1668. [PubMed: 501394]

Sillito AM, Cudeiro J, Jones HE. Always returning: feedback and sensory processing in visual cortex and thalamus. Trends in Neurosci 2006;29:307–316.

Stevenson JA, Lund RD. A crossed parabigemino-lateral geniculate projection in rats blinded at birth. Exp Brain Res 1982;45:95–100. [PubMed: 6173253]

Tokunaga A, Otani K. Neuronal organization of the corpus parabigeminum in the rat. Exp Neurol 1978;58:361–375. [PubMed: 618753]

Wang SR. The nucleus isthmi and dual modulation of tectal neurons in non-mammals. Brain Res Rev 2003;41:13–25. [PubMed: 12505645]

Wang Y, Luksch H, Brecha NC, Karten HJ. Columnar projections from the cholinergic nucleus isthmi to the optic tectum in chicks *Gallus gallus*: a possible substrate for synchronizing tectal channels. J Comp Neurol 2006;494:7–35. [PubMed: 16304683]

Wang Y, Major DE, Karten HJ. Morphology and connections of nucleus isthmi pars magnocellularis in chicks *Gallus gallus*. J Comp Neurol 2004;469:275–297. [PubMed: 14694539]

Wang Y, Xiao J, Wang SR. Excitatory and inhibitory receptive fields of tectal cells are differentially modified by magnocellular and parvocellular divisions of the pigeon nucleus isthmi. J Comp Physiol A 2000;186:505–511. [PubMed: 10947232]

Williams B, Hernandez N, Vanegas H. Electrophysiological analysis of the teleostean nucleus isthmi and its relationship with the optic tectum. J Comp Physiol A 1983;152:545–554.

Wilson ME, Toyne MJ. Retino-tectal and cortico-tectal projections in *Macaca mulatta*. Brain Res 1970;24:395–406. [PubMed: 4099749]

Xiao J, Wang Y, Wang SR. Effects of glutamatergic, cholinergic and GABAergic antagonist on tectal cells in toads. Neurosci 1999;90:1061–1067.

Yu CJ, Debski EA. The effects of nicotinic and muscarinic receptor activation on patch-clamped cells in the optic tectum of *Rana pipiens*. Neurosci 2003;118:135–144.

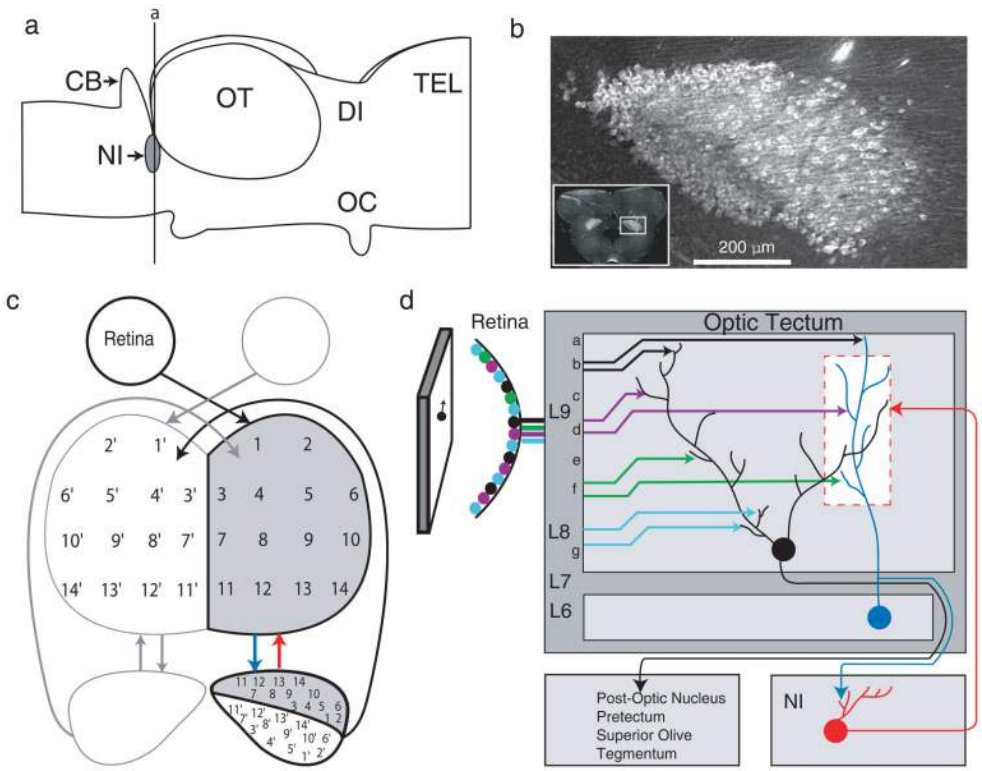

Fig. 1.

(color online) Nucleus isthmi and schematic of retino-isthmo-tectal system. **a** Lateral view of the brain. NI is ventral to the caudal pole of the tectum. Rostral is to the right. CB, cerebellum; DI, diencephalon; OC, optic chiasm; TEL, telencephalon. Transverse section a is shown in Fig. 1b inset **b** Fluorescent image of choline acetyltransferase-stain of NI magnified from inset (courtesy of Paul Gray). **c** Diagram of connectivity between retina, tectum and NI. Each eye projects a retinotopic map directly to the contralateral OT. The OT in turn projects (blue arrow) to cells in the NI. The numbered areas in the NI correspond to clusters of cells projecting to numbered areas in the OT. Dorsolateral NI cells (shaded) project (red arrow) to the ipsilateral OT. Ventromedial NI cells (not shaded) project to the contralateral OT (Figure adopted from Dudkin et al. 2007). **d** Diagram of ipsilateral retino-tecto-isthmal system. Four retinal ganglion axon types (black, green, purple and light blue arrows) enter lamina b,d,f and g and terminate in lamina a, c, e and f within layer 9 of the OT. They synapse onto dendrites of neurons whose cell bodies are located in layer 6 (blue) or layer 8 (black). NI cells (red) receive inputs from layer 6 axons, and project back to the column (white box) in the OT from which they receive inputs

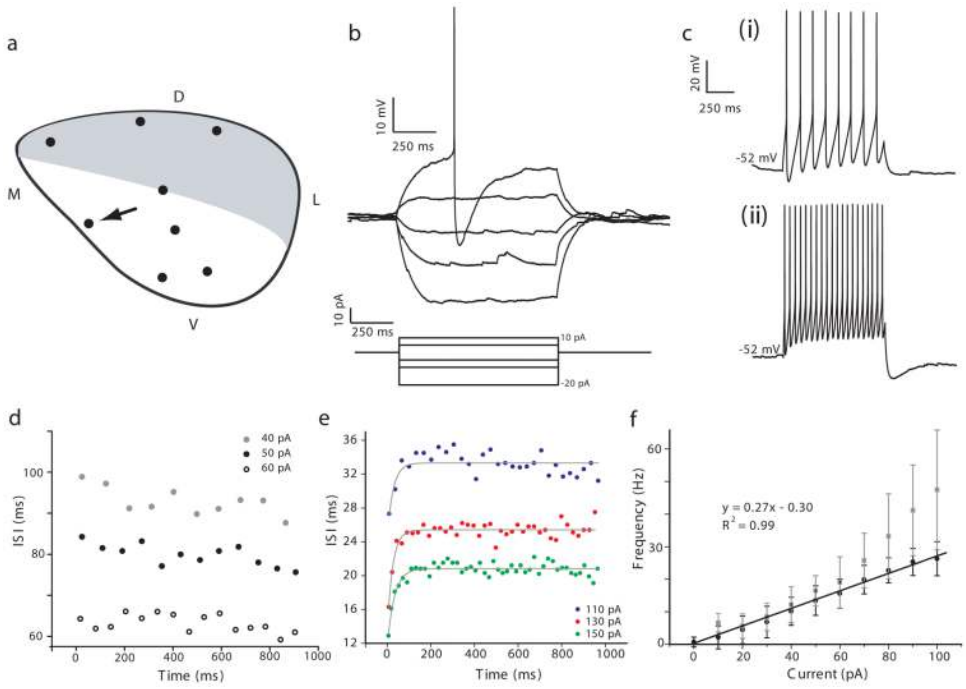

Fig. 2.

(color online) Electrophysiological properties of frog NI neurons. **a** Approximate recording sites of 8 NI neurons. D dorsal; L, lateral; V, ventral; M, medial. Arrow points to the cell whose data is presented in b–e. **b** Responses of NI neuron to small hyperpolarizing and depolarizing current injections. Note: monophasic AHP. **c** (i,ii) Responses of cell denoted by arrow in (a) to two current injections above rheobase. All the cells responded with similar tonic discharge patterns for the 1-second duration current pulse. **d** At low current injections (60 pA) the interspike intervals show no spike-rate adaptation. **e** Higher current injections cause significant spike-rate adaptation. Grey lines are exponential fits to the data. **f** Current to spike frequency relationship (n = 8cells) is linear (filled black circles) for currents up to 100 pA. The instantaneous frequency (solid grey squares) measured as the inverse of the first ISI is nonlinear for currents exceeding 60 pA

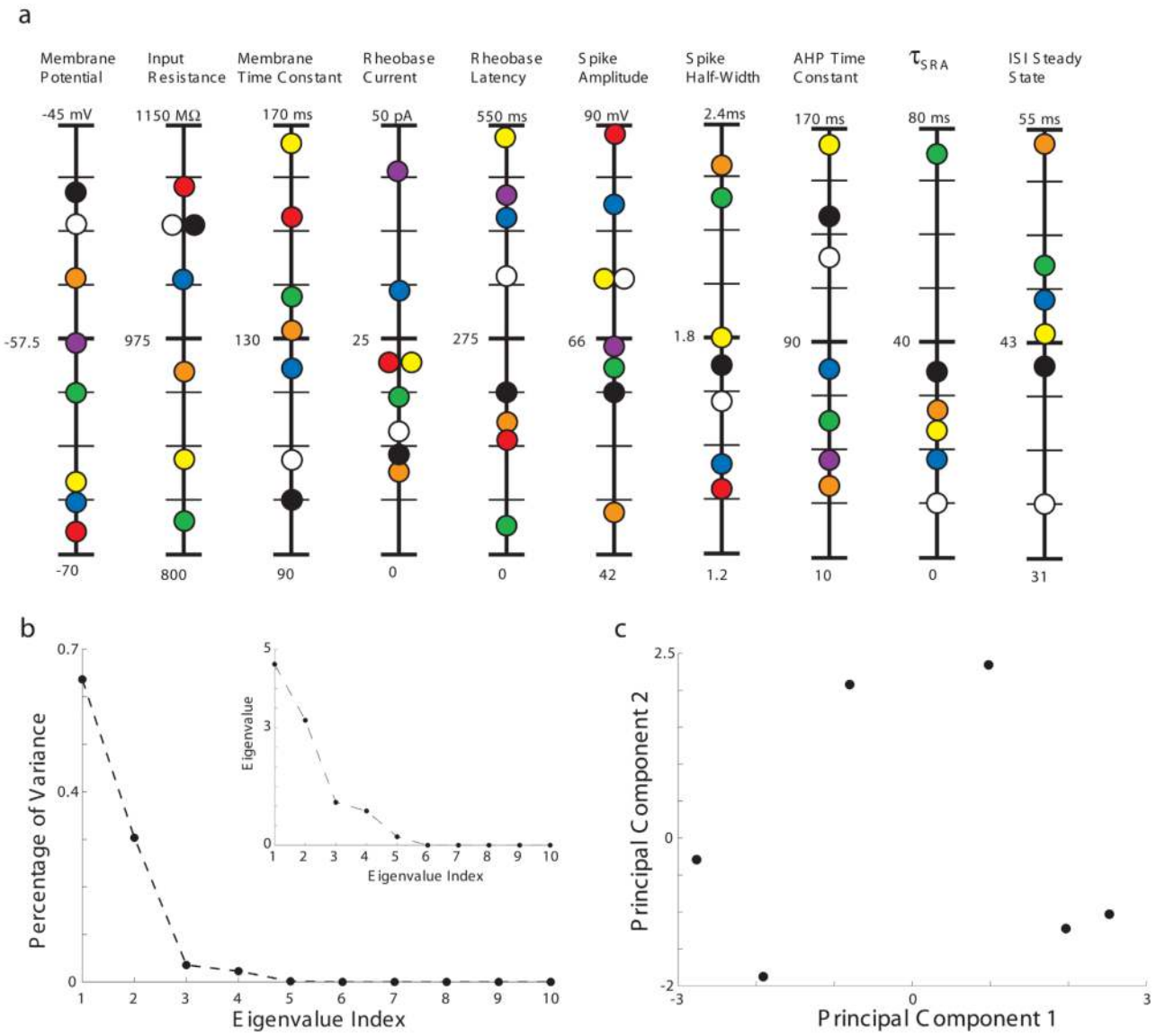

Fig. 3.

(color online) Principal component analysis of the cellular properties of NI neurons. **a** Ten different measurements taken from each cell are plotted in separate columns. Colored circles represent individual cells. Note: for some measurements only 6 or 7 cells contributed. **b** Eigenvalues determined by a principal component analysis of the 6 cells that appear in all 10 columns of A are shown in the inset. The larger figure shows that the first two eigenvalues account for >90% of the data's variance. This motivates the choice to keep only two principal components (eigenvectors). **c** Projection of standardized measurements in a onto the principal components corresponding to the largest two eigenvalues in b is distributed about the mean values (standardized to be 0). Thus, no discrete clusters are apparent for these 6 cells in the 2-dimensional principal component space

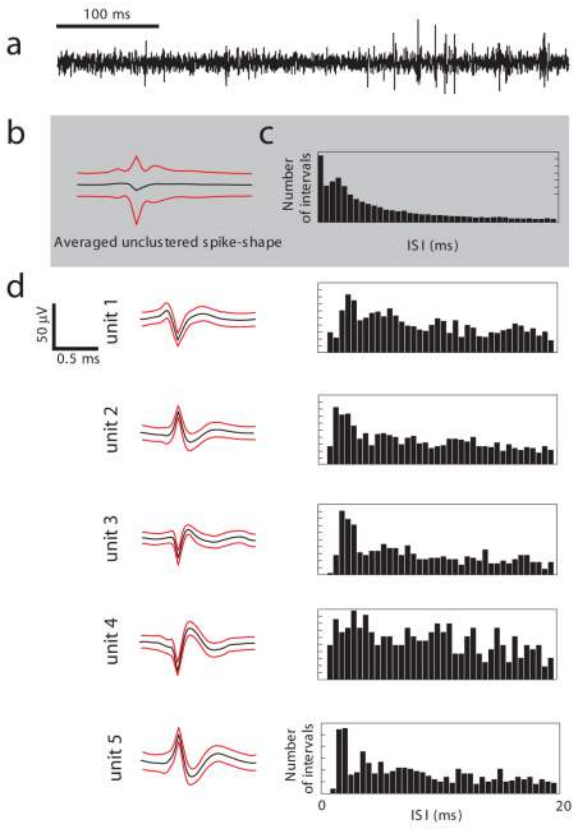

Fig. 4.

(color online) Sorted spike shapes and associated ISI distributions obtained from one recording site in response to steps in diffuse illumination. At this recording site, there were 72563 detected spikes. **a** Representative voltage traceof spontaneous activity **b** Average spike shape of the unsorted response to diffuse illuminationwith standard deviations (red). **c** Interspike interaval distribution of unsorted response to diffuse illumination with intervals less than 1ms. **d** Five units obtained after spike sorting and the corresponding ISI distributions. No sorted units have an ISI of less than 1 ms

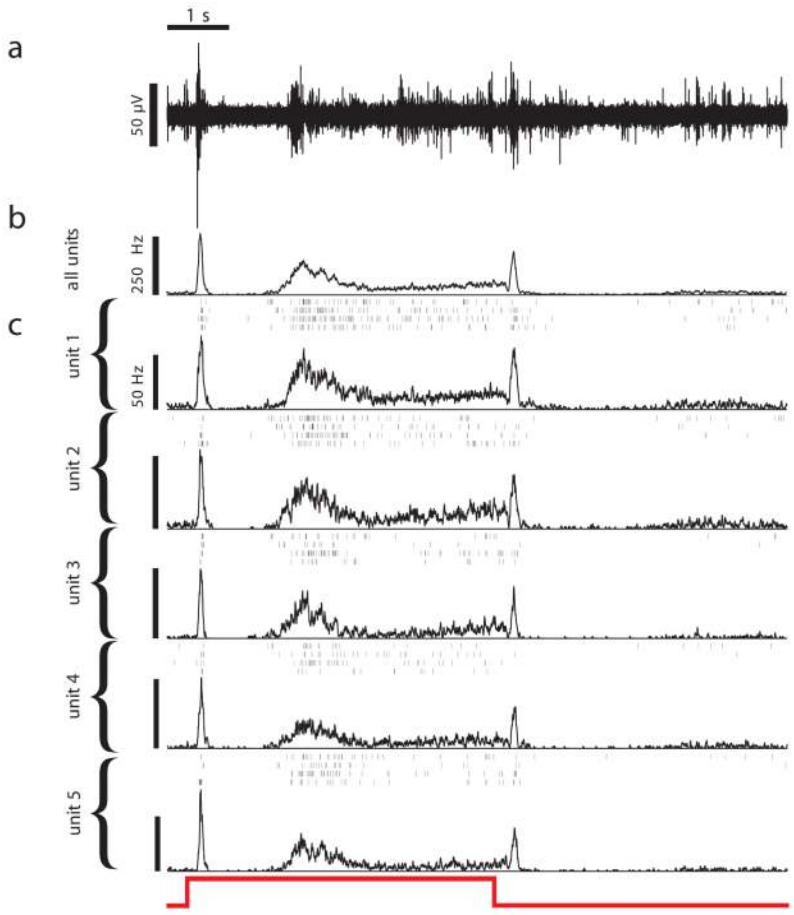

Fig. 5.

(color online) Sorted responses to a 5-second step in diffuse illumination. Recording site is the same as in figure 4. **a** Sample voltage trace of multi-unit activity. **b** Multi-unit average firing rate obtained from 50 trials (only four raster plots are shown for clarity). **c** Five single-unit average firing rate plots based on 50 trials (only four raster plots are shown for clarity). Scale bar in all single-unit average firing rate plots is 50 Hz. The red curve is the time course of the stimuli

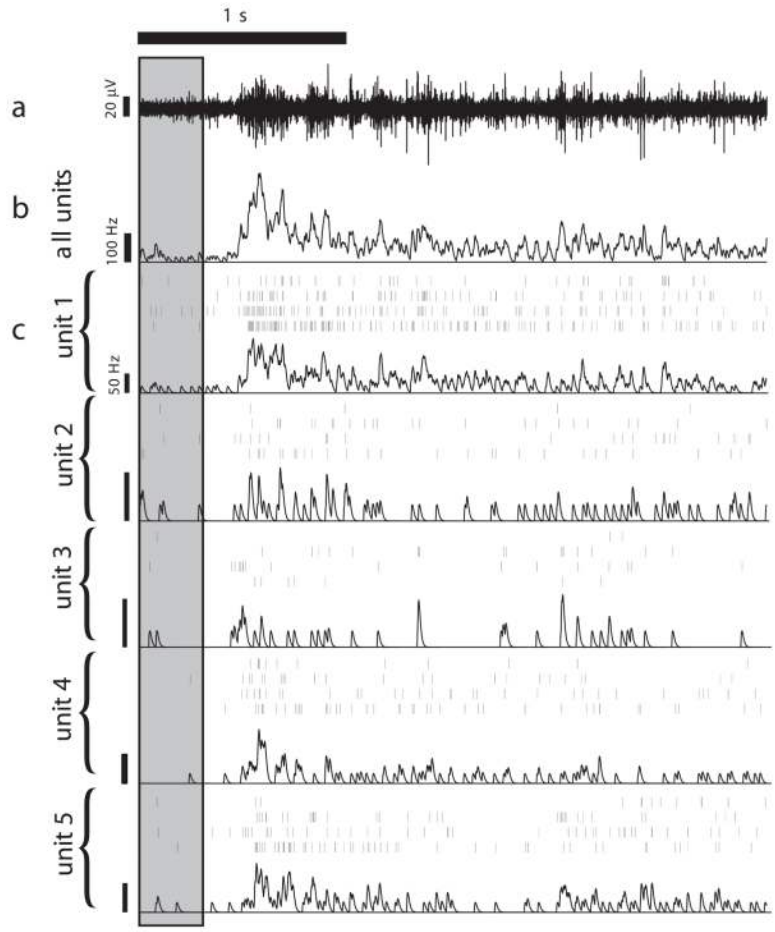

Fig. 6.

(color online) Sorted responses to the commencement of motion of a 15-degree moving black spot. **a** Sample voltage trace of multi-unit activity. **b** Multi-unit average firing rate for four trials. The spot moved in the temporal-nasal direction at 10 deg/s. **c** Five sorted single-unit average firing rate plots based on four trials. Scale bar in all single-unit average firing rate plots is 50 Hz. The shaded section denotes the time before the spot started moving

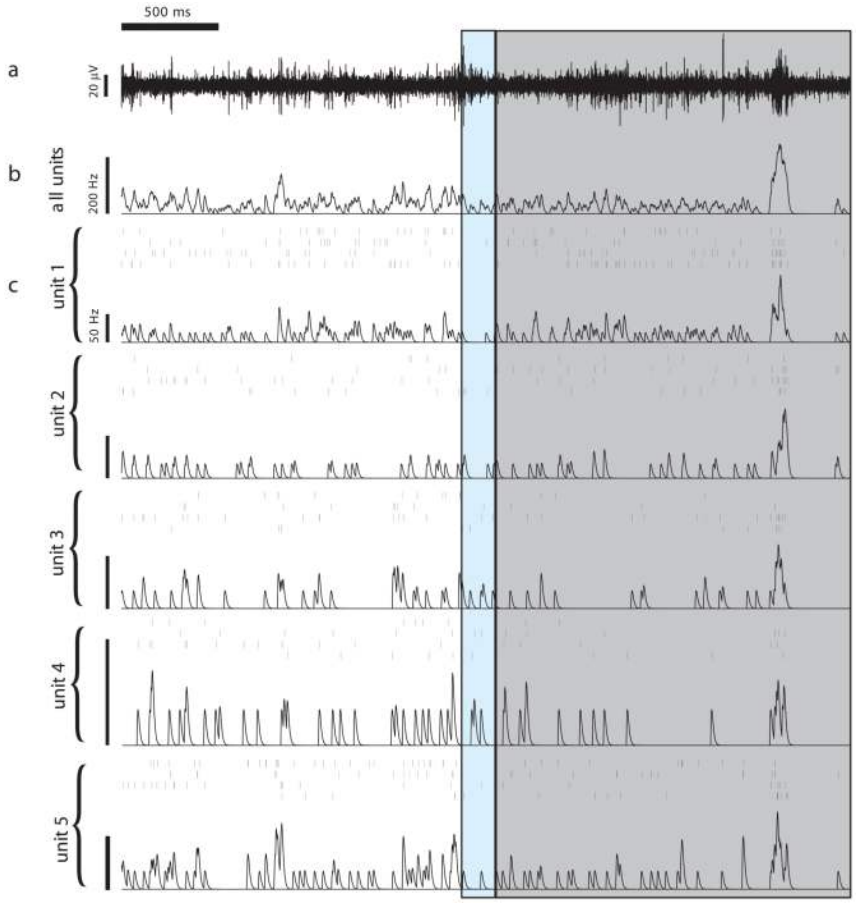

Fig. 7.

(color online) Sorted responses to the cessation of the motion of the 15-degree spot for the five units shown in figure 6. **a** Sample voltage trace of multi-unit activity. **b** Multi-unit average firing rate for four trials. **c** Five sorted single-unit average firing rate plots based on four trials. Scale bar in all single-unit average firing rate plots is 50 Hz. The white section denotes spot movement. At the start of the blue section, the spot stopped moving. The width of the blue section corresponds to the typical latency for a response to a visual stimulus. The blue and shaded sections denote that the spot is stationary. Approximately 1700 ms after the spot ceased moving, a transient increase in the firing rate occurs in all 5 units

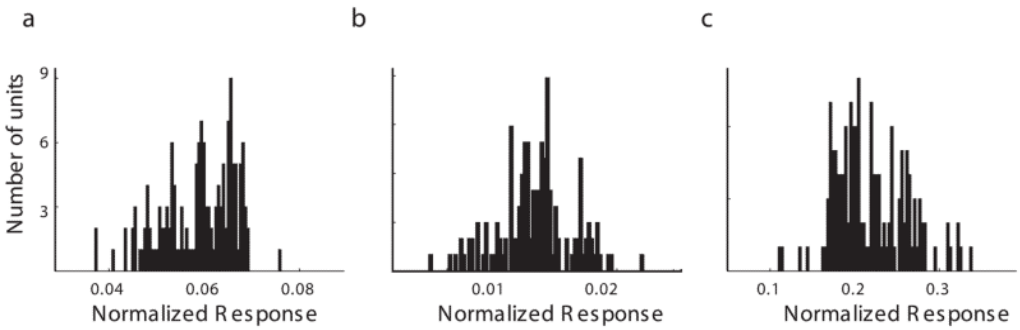

Fig. 8.

Histogram distributions of normalized salient responses. **a** Responses to the commencement of motion of a moving-spot in the visual field. **b** Delayed response to the cessation of a moving-spot. **c** Initial transient response to diffuse illumination

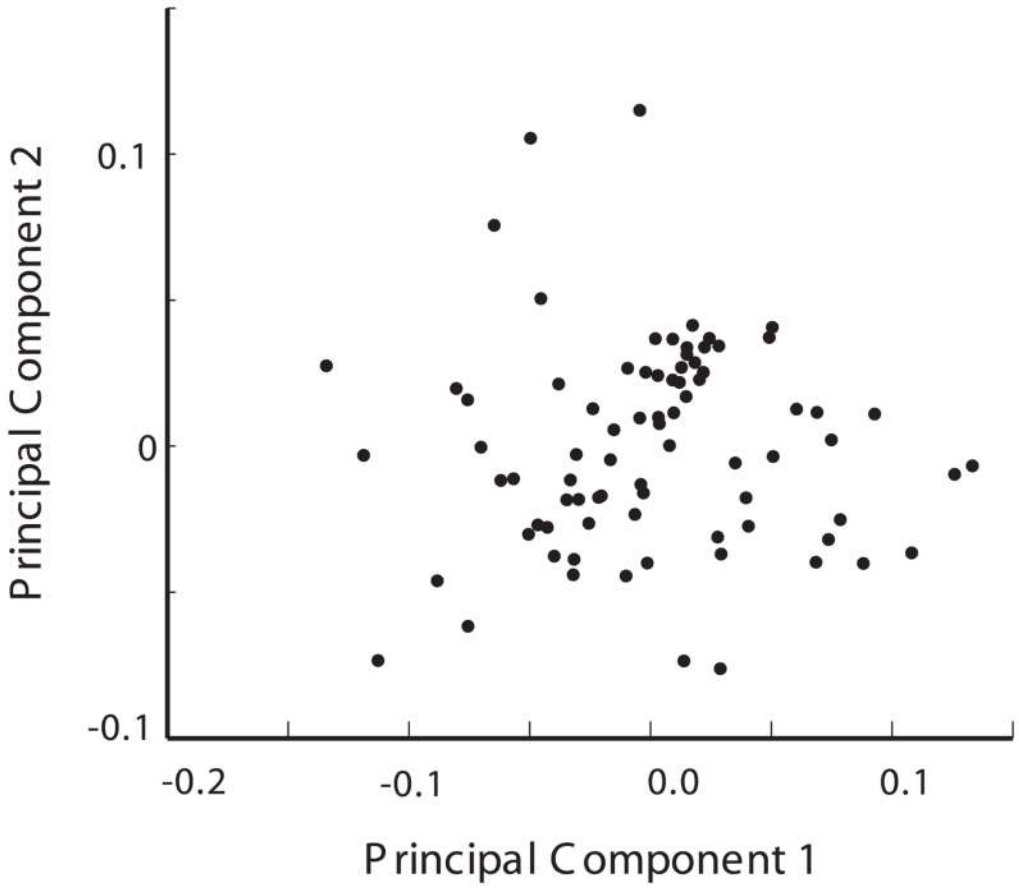

Fig. 9.
Projection of principal component scores onto the plane of the first two principal components. Note the lack of any distinction between clusters